https://doi.org/10.3311/PPci.23514

Periodica Polytechnica Civil Engineering

Optimization of H-type Anti-slide Pile Support Structure Based on RSM-NSGA-II

Yousheng Deng[1], Keqin Zhang[1*], Biao Yang[1], Long Li[1], Huiling Zhao[1], Zhigang Yao[1]

[1] School of Architecture and Civil Engineering, Xi'an University of Science and Technology, 58 Yanta Road, 710054 Xi'an, China
[*] Corresponding author, e-mail: zhangkq321@163.com

Received: 25 September 2023, Accepted: 01 June 2024, Published online: 25 June 2024

Abstract

The parameters of an h-type anti-slide pile are optimized and analyzed with respect to its structural characteristics. Based on laboratory model tests, further analysis of its stress characteristics is carried out through numerical simulation methods. Then, the response surface methodology (RSM) combined with the NSGA-II algorithm was employed to perform multiobjective optimization of the reinforcement performance and engineering cost for h-type anti-slide piles regarding landslide consideration. Finally, the entropy weight TOPSIS method was used for comprehensive evaluation to obtain the optimal structural parameters. The results show that the bending moment distribution of the front and rear rows of h-type piles first increases and then decreases with increasing depth, and the front soil pressure of the pile gradually increases. Using RSM-NSGA-II instead of finite element modeling can shorten the optimization time, and the accuracy of the surrogate model reaches 94.8%. NSGA-II is much stronger than that of the particle swarm optimization algorithm. The entropy weight method combined with the TOPSIS method can obtain the unique optimal solution from the Pareto solution set without prior knowledge. The h-type anti-slide pile with the best structural parameters reduces the cost by 75.19%, while the slope safety factor increases by 47.39%. This method provides a new idea for structural optimization.

Keywords

h-type anti-slide pile, response surface methodology, NSGA-II, TOPSIS method, model test, numerical simulation

1 Introduction

Due to the complex terrain and geomorphological environment, there are a large number of slopes with thick overlying soil layers and steep slopes in the western region of China, which are prone to landslide disasters along weak interfaces [1]. With the continuous development of railway projects in China, it is difficult for railways to bypass the adverse geological conditions in the western region. Therefore, the stability of the embankment must be guaranteed during construction. As a result, anti-slide piles have been widely used to mitigate landslide issues [2]. Although anti-slide piles have good supporting effects, their structure is simple, and there is significant displacement at the pile top, with a relatively narrow construction face [3]. In recent years, the structural forms of anti-slide piles have been continuously optimized, resulting in the emergence of mini anti-slide piles [4], spatial arc-shaped anti-slide piles [5], gantry-type anti-slide piles, etc. [6]. The h-type anti-slide pile is a structural improvement of the gantry-type anti-slide pile [7]. It arranges two unequal-length anti-slide piles parallel to each other, connecting the top of the front pile with a certain position of the back pile through a beam. The rear row of piles has a cantilevered section for spatial support. Due to its resemblance to the lowercase letter "h", it is called an h-type anti-slide pile [8].

In recent years, the h-type anti-slide pile has been applied in many engineering projects. However, many of its structural parameters are set based on empirical experience. It is necessary to optimize and analyze these structural parameters. Li et al. [9] conducted indoor model tests and found that a smaller cantilever section length of the h-type anti-slide pile leads to a larger horizontal displacement at the pile top, and the optimal length of the connecting beam is 5 times the cross-sectional diameter of the pile. Liu et al. [10] analyzed the influence of different beam stiffnesses and anchorage depths through model tests and numerical simulations. They found that when the sliding surface is small, the length of the connecting beam should

Cite this article as: Deng, Y., Zhang, K., Yang, B., Li, L., Zhao, H., Yao, Z. "Optimization of H-type Anti-slide Pile Support Structure Based on RSM-NSGA-II", Periodica Polytechnica Civil Engineering, 2024. https://doi.org/10.3311/PPci.23514

be 9 times the pile diameter, and when the sliding surface angle is large, the length of the connecting beam should be 5 times the pile diameter, with the anchorage depth of the front pile greater than that of the back pile. Details on the h-type anti-slide pile research process are shown in Table 1. Most existing studies have focused on optimizing the beam structure parameters, and the optimization process only considers single-factor effects. However, in practical structural work, multiple factors simultaneously influence the performance. Therefore, this study adopts the response surface methodology (RSM) to establish an RSM model that investigates the effects of various structural parameter variations on response values, aiming to consider a multifactor approach to structural optimization.

In engineering, cost is an essential factor to consider, and there have been numerous studies on the structural optimization problem that aim to minimize cost while ensuring structural performance. Deng et al. [14] conducted a three-objective optimization of the beam-pile structure considering cost, load-bearing capacity, and work efficiency using a genetic algorithm, achieving good results. Tang et al. [15] and Yao et al. [16] both performed multiobjective optimization analyses based on reinforcement efficiency and cost efficiency for the diameter, pile length, pile spacing, and pile position of anti-slide piles. In this study, the influence of cost is fully taken into account, and a multiobjective optimization model considering cost and slope safety factors is established using the advanced NSGAII algorithm [17] in the genetic algorithm. The optimal combination of structural parameters is obtained by integrating the entropy weight method with the TOPSIS (Technique for Order Preference by Similarity to Ideal Solution) method for comprehensive evaluation.

Table 1 Major research processes for h-type anti-slide pile

Year	Author	Major contribution	Ref. No.
2012	Ou et al.	First study of h-type anti-slide pile.	[7]
2017	Luo et al.	In-situ experimental studies were conducted.	[8]
2017	Zhao et al.	Analyze the differences between the performance of h-type anti-slide pile and other structures.	[11]
2018	Liu et al.	Some design suggestions of h-type anti-slide pile are proposed.	[10]
2022	Zhao et al.	Proposing an improved calculation method for the internal force of h-type anti-slide pile.	[12]
2022	Li et al.	Modeling of h-type anti-slide piles with curved sliding surfaces.	[9]
2023	Zhang et al.	A centrifuge model test was conducted.	[13]

This study focuses on h-type anti-slide pile, establishing a numerical model using finite element analysis and validating its mechanical properties through experimentation. It analyzes the impact of various structural parameters on slope reinforcement effectiveness and cost, utilizing the RSM model and NSGA-II algorithm to identify optimal structural parameters, providing guidance for engineering application and optimization.

2 Model test and numerical simulation

2.1 Model test

A reduced-scale indoor model test was conducted based on the actual slope condition in Wuqi County, Shaanxi Province, China. The experiment is based on the principle of similarity, with geometric dimension similarity ratio (C_L) as the first fundamental quantity, gravity similarity ratio (C_γ) as the second fundamental quantity, and strain similarity ratio (C_ε) as the third fundamental quantity. By using these three fundamental quantities as a basis, other variables' similarity ratios can be derived, as shown in the Similarity column in Table 2.

The experimental slope was divided into three parts: sliding mass, sliding surface, and sliding bed. The sliding mass was composed of natural loess and compacted in layers. The sliding surface was designed as an arc shape and simulated using plastic film. Because the prototype slope we tested did not experience sliding failure, we couldn't determine its actual sliding surface. To obtain a more realistic sliding surface, we employed the strength reduction method in ABAQUS to analyze the prototype slope without pre-defined sliding surfaces, as shown in Fig. 1. Based on these results, the predetermined sliding surface was determined for the model test. The physical parameters of the sliding zone were calculated based on the loading conditions at the limit equilibrium state of the landslide [18], resulting in a cohesive force of 14.8 kPa and an internal friction angle of 13.1°.

The h-type anti-slide piles consisted of long piles (rear piles) with a length of 700 mm and short piles (front piles) with a length of 500 mm. The design spacing between

Table 2 Similarity ratio design

Physical quantity	Similarity	Similarity ratio (Prototypes: Models)
Geometric dimension/L	C_L	10:1
Weight/γ	C_γ	1:1
Stress/σ	$C_\sigma = C_L C_\gamma$	10:1
Strain/ε	C_ε	1:1
Displacement/δ	$C_\delta = C_L C_\varepsilon$	10:1

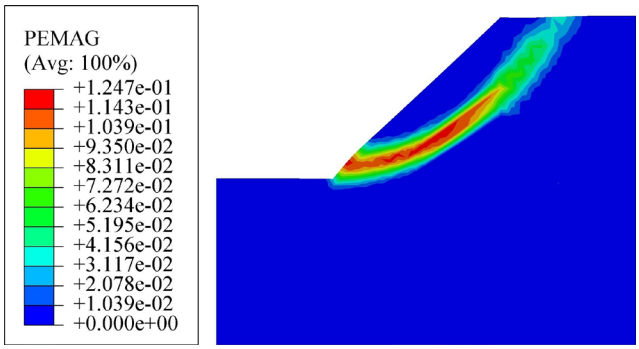

Fig. 1 Diagram of landslide location

piles was 150 mm, and the row spacing was also 150 mm. The front and rear piles were connected by a middle beam through welding. The front piles of the anti-slide piles were arranged at the middle position of the slope, which had a slope angle of 45°. The measurement system included a YTDZ0301 soil pressure cell, BF1K-3EB full-bridge strain gauges, and Donghua DH3816 stress-strain data acquisition instruments for collecting data on the soil pressure in front of the piles and the internal forces of the piles. The test was conducted using a slow and incremental loading method, with a single-level load of 28.4 kPa and eight levels gradually increasing to 227.2 kPa. The schematic diagram of the test process is shown in Fig. 2, and the layout diagram of the test is shown in Fig. 3. The parameters of the soil and piles were obtained through measurements, as shown in Table 3.

2.2 Numerical simulation

A numerical simulation model was established using ABAQUS, with dimensions ten times larger than the model test. The piles were defined as elastic, and the soil was modeled using the Mohr–Coulomb constitutive model. The parameters for the soil and piles were set based on the measured values from the model test. Frictional contact between the soil and piles was defined using "hard" contact and a penalty function, with a friction coefficient of 0.25. To prevent rigid body movement in the simulation, the normal displacement of the soil surrounding the model and at the bottom was set to zero. The model was incrementally loaded eight times to 227.2 kPa after achieving stress equilibrium at the slope crest. The mesh division of the model is shown in Fig. 4.

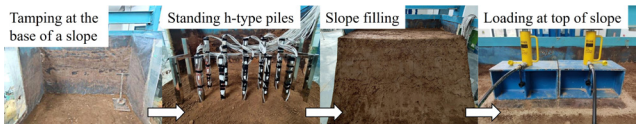

Fig. 2 Model test process

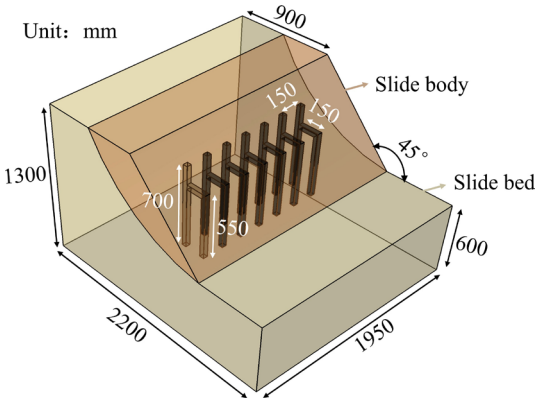

(a)

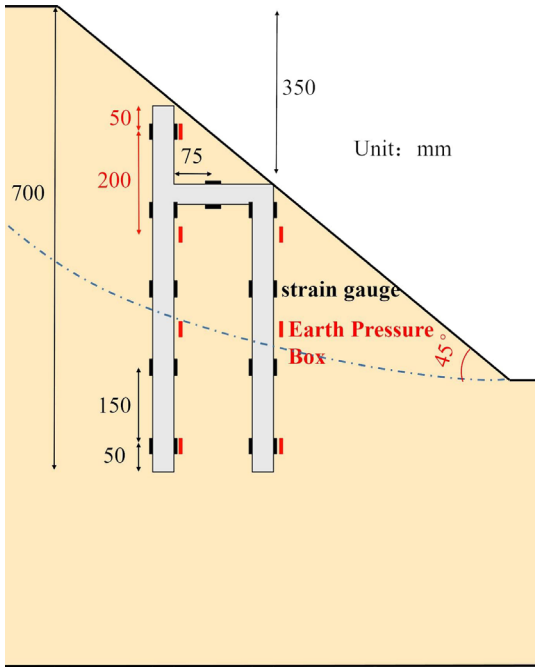

(b)

Fig. 3 Model test layout; (a) Model size diagram; (b) Location of the earth pressure box and strain gauge

Table 3 Material parameters

	Weight/ (kN/m³)	Cohesive/ kPa	Friction angle/°	Poisson's ratio	Elastic modulus/MPa
Loess	20.8	32.5	30.05	0.32	16.38
Pile	24.0	–	–	0.20	3×10^4

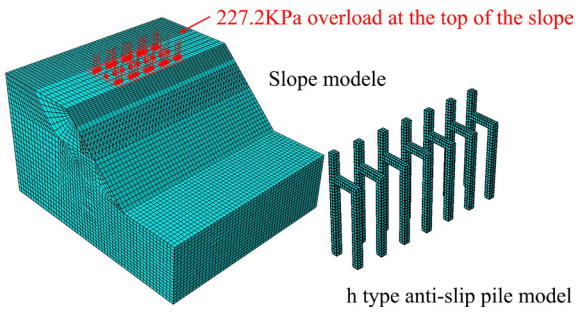

Fig. 4 Finite element mesh division

2.3 Model validation

The model test data were compared and analyzed with the numerical simulation results (see Fig. 5). The research objective of this paper is the h-type anti-slide pile; therefore, the focus was mainly on comparing the forces acting on the pile body. The overall trend observed in the model test was consistent with the numerical simulation results, which verified the accuracy of the finite element model and provided guidance for further numerical analysis.

The bending moment distribution along the pile body is shown in Fig. 5(a). The numerical simulation results indicated that the bending moment of the rear piles followed an "inverse S-shaped" distribution along the height of the pile, with the inflection point located at a distance of 5.5 m from the pile bottom, i.e., the upper part near the connection beam. This suggests that under the load at the slope crest, the bending moment at the top of the rear piles tends to approach zero. Due to limitations in the experimental conditions, strain gauges were not installed at the top of the piles in the model test. As a result, the observed bending moment values near the pile top tended to be positive and gradually increased. For the front piles, under the load at the slope crest, the bending moment along the height of the front piles initially increased and then decreased. It reached its maximum value at a position approximately 1.5 m below the pile top, and the bending moment at the pile bottom approached zero, but it was not zero at the pile top. The model test results were close to the numerical simulation, although the bending moment value at the pile top was missing.

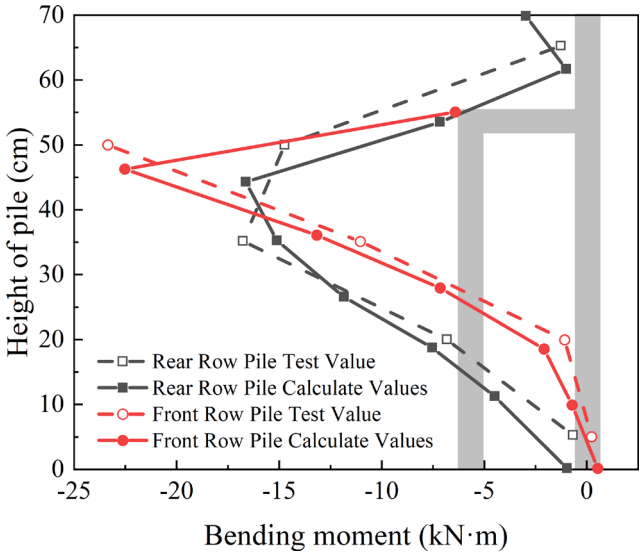

(a)

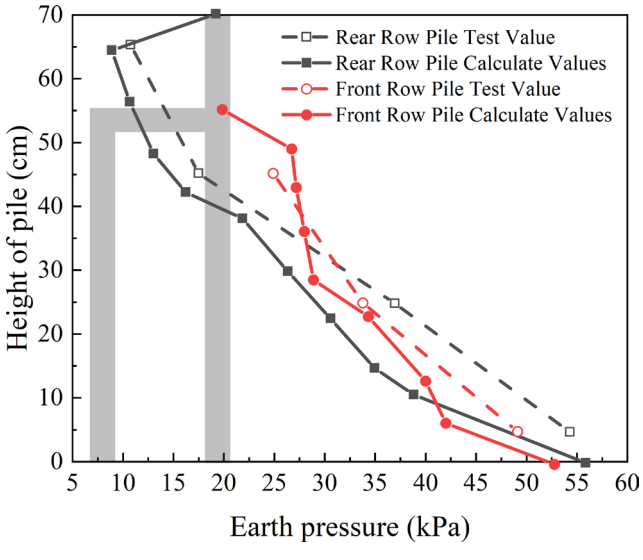

(b)

Fig. 5 Comparison of the test and finite element results; (a) Pile bending moment; (b) Soil pressure before pile

The comparison analysis of soil pressure is shown in Fig. 5(b). The soil pressure in front of the rear piles showed a trend of decreasing and then increasing with increasing pile height. At a section approximately 0.5 m below the top of the rear piles, the soil pressure in front of the piles approached zero, and it reached its peak value at the section at the pile bottom. The variation in soil pressure in front of the piles was significant within a certain range both below the pile top and above the pile bottom. As the soil in front of the piles is relatively thick and stable, it can provide greater soil resistance, and the deeper the pile is, the higher the self-weight of the soil. Therefore, a peak soil pressure appears near the pile bottom. This pattern was not observed in the model test, as pressure cells were not installed at the pile top and bottom. In the case of the front piles, due to the limited number of measuring points in the model test, the soil pressure curve showed a smooth and approximately linear distribution. However, the numerical simulation results revealed that the soil pressure in front of the piles at the pile top approached zero due to the thinner soil layer, increased uniformly along the pile from the top to the bottom, and experienced a sudden change at a distance of 0.8 m from the pile bottom, reaching its maximum value at the pile bottom.

3 Univariate analysis

Combining the analysis above with relevant literature studies [8–13], both the front and rear row piles, as well as the beam structure of the h-type anti-slide pile, effectively contribute to the anti-slide function. Therefore, seven structural parameters of the h-type anti-slide pile were selected for analysis, including the beam connection

length (H_{CB}), cantilever section length (H_{PB}), rear pile length (H_{BP}), front pile length (H_{FP}), beam stiffness (E_{CB}), rear pile stiffness (E_{BP}), and front pile stiffness (E_{FP}), as shown in Fig. 6. The structural parameters from indoor model tests were taken as reference values for single-factor analysis. When considering the effect of one parameter, with the remaining parameters kept constant at the reference values, as shown in Table 4. The main objective of optimization is to increase the slope stability coefficient *FS* and reduce construction costs. Numerical models corresponding to different structural parameters were established, and the strength reduction method was used to calculate the corresponding *FS*.

The h-type anti-slide pile is a combination of reinforced concrete piles and beams, and the cost considerations should include concrete strength grade and amount of reinforcement. The parameter selection fully considers the influence of the pile and beam modulus of elasticity, which reflects the rigidity of the materials. It can be used as an important reference for selecting the concrete strength grade and reinforcing bar ratio. To simplify the calculations, the cost (ω') is defined as the product of the volume and modulus of elasticity [14], as shown in Eq. (1). To eliminate the difference in magnitude between the volume and modulus of elasticity, they need to be normalized before calculation.

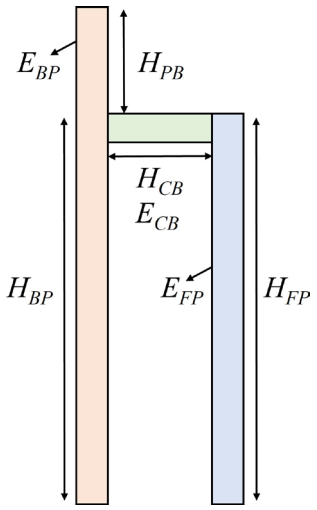

Fig. 6 Schematic diagram of structure parameter selection

$$\omega' = AE + (B + C)F + DG \tag{1}$$

where $A \sim G$ represent the code names of various structural parameters in Table 4.

The stability and cost of the slope are influenced by the structural parameters, as shown in Fig. 7.

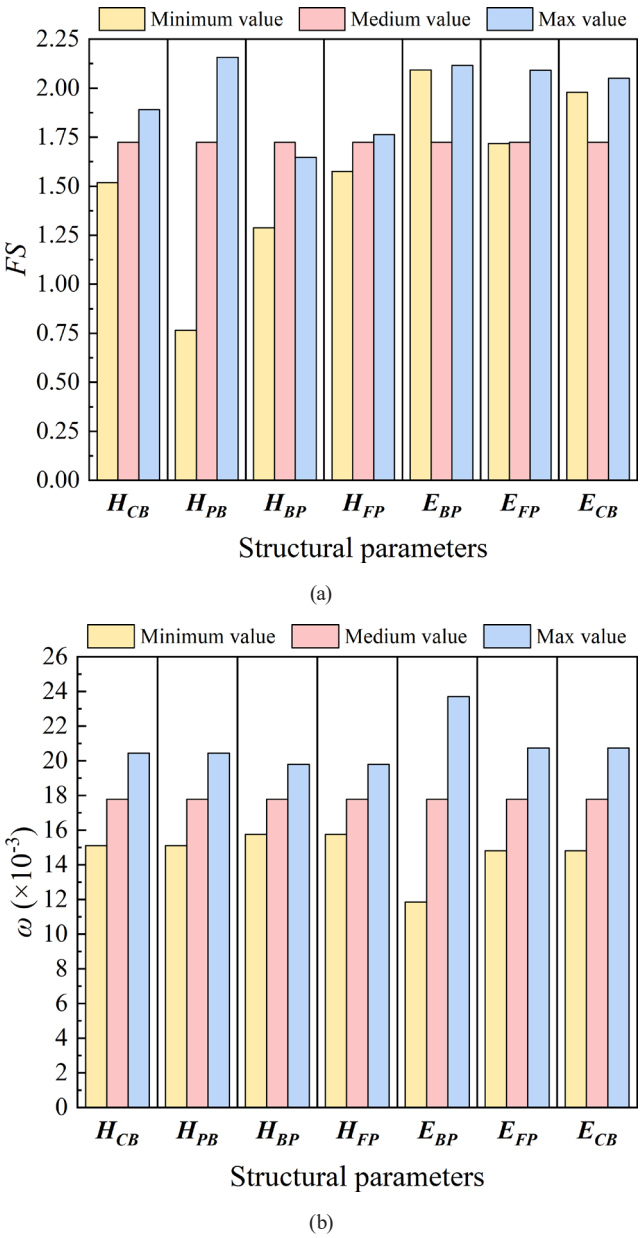

Fig. 7 Influence of different structural parameters; (a) Slope stability; (b) h-type pile cost

Table 4 Structural parameters

Structural parameters	H_{CB}/m	H_{PB}/m	H_{BP}/m	H_{FP}/m	E_{BP}/MPa	E_{FP}/MPa	E_{CB}/MPa
Code name	*A*	*B*	*C*	*D*	*E*	*F*	*G*
Minimum value	0.6	0.6	3.0	3.0	1×10^4	1×10^4	1×10^4
Reference value (median)	1.5	1.5	5.5	5.5	3×10^4	3×10^4	3×10^4
Max value	2.4	2.4	8.0	8.0	5×10^4	5×10^4	5×10^4

Different structural parameters have significant differences in their impact on slope stability. Among them, the length of the cantilever section (H_{PB}) has the greatest influence on the *FS*. When the length is small, the h-type anti-slide pile cannot effectively reinforce the slope, resulting in a safety factor of less than 1, indicating that the slope is in an unstable state. However, as the length of the cantilever section increases, the safety factor significantly improves, reaching 2.16. The length of the beam (H_{CB}) and the length of the front row piles (H_{FP}) also have a significant impact on the safety factor, which increases with increasing length. This finding is in line with literature [10, 11]. On the other hand, when the length of the rear row piles (H_{BP}) is too long, the reinforcement effect decreases, indicating that the anchor depth of the rear row piles affects the anti-slide effect of the h-type pile.

The stiffness of the front and rear row piles and the beam does not have a linear distribution in terms of its impact on the safety factor. When the stiffness of the rear row piles and the beam is relatively low, the reinforcement effect on the slope is still significant, almost similar to the effect when the stiffness is high. This is because the stiffness of the two piles is almost the same, resulting in better stiffness matching [9]. On the other hand, the stiffness of the front row piles has a relatively average reinforcement effect at lower stiffness, but it yields a higher safety factor at a stiffness of 5×10^4 MPa due to the increased bending moment it bears [13].

Therefore, the order of influence of the parameters of the h-type anti-slide pile on the bearing capacity from largest to most minor is $H_{PB} > H_{BP} > H_{CB} > E_{FP} > E_{BP} > H_{CB} > H_{FP}$.

The cost increases as the structural parameters of the h-type anti-slide pile increase, and the impact trends of different structural lengths on cost are generally consistent. According to Eq. (1), it can be observed that the stiffness of the rear row piles (E_{BP}) needs to match both the length of the rear row piles and the length of the cantilever section, making it the parameter with the greatest impact on cost. When its value is small, the required cost is minimal, while for higher values, the corresponding cost is maximum. Therefore, this parameter needs to be carefully considered during the optimization process.

4 Optimization method

4.1 Method introduction

RSM is a commonly used experimental design and analysis method that focuses on response variables. It establishes mathematical models to describe the relationship between response variables and input factors, facilitating design and analysis. RSM consists of three main steps: experimental design, modeling, and statistical analysis. Experimental design obtains efficient data through appropriate sampling strategies and scheme settings, while the modeling stage maps the data to mathematical models based on regression analysis, exploring the relationship between response variables and input factors. The statistical analysis verifies the established mathematical models. The characteristics of RSM include efficiency, reliability, ease of operation, and interpretability, making it widely applied to various optimization tasks [19].

Considering the need to consider nonlinear situations, this study employs second-order RSM, as shown in Eq. (2), as a universal model:

$$Y = \beta_0 + \sum_{i=1}^{k} \beta_i X_i + \sum_{i=1}^{k} \beta_{ii} X_i^2 + \sum_{i=1}^{k-1} \sum_{i=j+1}^{k} \beta_{ij} X_i X_j + \varepsilon, \qquad (2)$$

where Y represents the predicted response value (*FS*, ω); X_i represents the independent variables; β_0 is a constant; β_i, β_{ii}, and β_{ij} are coefficients; and ε denotes the error term.

NSGA-II is a fast nondominated sorting genetic algorithm with an elitism strategy. It stratifies the population based on the noninferior level of individuals while considering the crowding distance calculation and elitism strategy. Adopting the crowding distance comparison operator reduces the computational complexity of the algorithm and avoids local convergence during the optimization process [20]. The basic procedure of NSGA-II is as follows: First, in the initialization stage, a random initial population is created. Then, based on the nondominated sorting strategy and crowding distance operator, a portion of the population is selected as candidate solutions for the next generation. New solutions are generated through crossover and mutation and added to the candidate solution set. Finally, the candidate solution set is sorted and filtered using the nondominated sorting strategy and crowding distance operator to generate the next generation population.

The entropy weight method is a multiattribute decision-making analysis method aimed at determining the weights of each attribute. Its basic idea is to measure the uncertainty level relative to the ideal state using entropy values and calculate the weight of each attribute [21]. The entropy weight method does not require any prior knowledge and only relies on the information of the data itself, ensuring more objective weight determination.

TOPSIS is a multiattribute decision-making analysis method. The steps involved are as follows: First, the decision matrix needs to be defined, which arranges the candidate solutions into a matrix according to different attributes. Then, the entropy weight method is used to determine the weights and identify the maximum and minimum values for each attribute as positive and negative ideal solutions. The distance from each solution to the positive and negative ideal solutions is calculated, and the ranking of the solutions based on their degrees of superiority is determined, resulting in the optimal solution. TOPSIS can simultaneously consider multiple factors, improving decision-making efficiency and accuracy [22].

4.2 Main process

Structural parameter optimization is a repetitive iterative process. Numerical simulation can alleviate the burden of extensive experiments by establishing numerous models and conducting calculations. However, as the accuracy requirements for simulations increase, it is common for the optimization process to become excessively time-consuming or even ineffective. To address this issue, this study utilizes numerical simulation combined with RSM to establish surrogate models for the relationship between structural performance and various parameters. Subsequently, during the search for the optimal results under multiple objectives using the NSGA-II genetic algorithm, the RSM model is employed instead of finite element calculations, significantly reducing computation time and enhancing optimization efficiency [23].

The main workflow of this study is illustrated in Fig. 8. The main workflow is as follows:

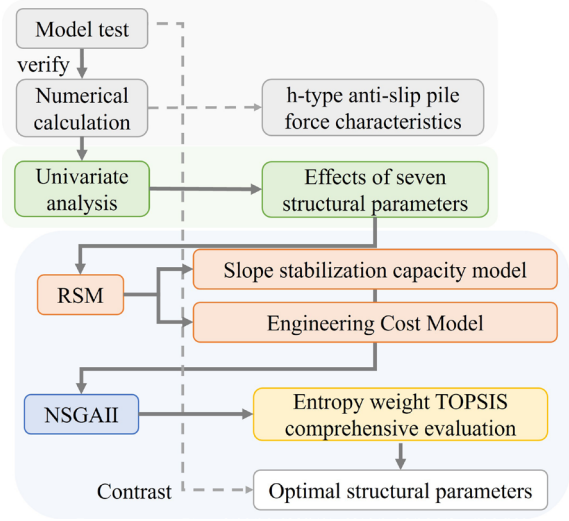

Fig. 8 Optimization of the technical route of the h-type anti-slide pile

1. We validated the accuracy of numerical calculations through model test and analyzed the force characteristics of h-type anti-slide piles.
2. Based on the parameter design univariate analysis of model test, we selected seven structural parameters and two dependent variables: slope stability coefficient and the cost of h-type anti-slide piles.
3. Two response surface models were established based on the structural parameters and dependent variables, and the slope stability coefficient was obtained through numerical calculations.
4. Based on the established response surface mathematical models, NSGA-II was used for multi-objective optimization. After obtaining the optimal solution set through the genetic algorithm, it is necessary to determine a unique optimal solution. This study adopts the entropy weight method to determine the weights corresponding to FS and ω. The TOPSIS method is then employed for a comprehensive evaluation to seek the ideal solutions within the Pareto optimal frontier.
5. Particle swarm optimization algorithm is added in the optimization algorithm section as a comparative analysis of the advantages of NSGA-II.

5 Results and discussion

5.1 RSM model

Since the use of Eq. (2) to calculate the cost of anti-slip piles requires the normalization of all parameters, which does not give better results when only a small amount of data is calculated or when the total number of data sets that need to be calculated cannot be predicted, the RSM method is used here to build a proxy model for it. Taking the parameters with strong sensitivity selected from Section 3 as independent variables, a seven-factor three-level RSM model correlating the slope stability coefficient FS with the cost ω of h-type anti-slide piles is established based on Table 3. The RSM experimental points are designed using Design-Expert software combined with the Box–Behnken experimental design method, resulting in a total of 62 sets of experiments. The FS values are obtained through numerical simulation, while the ω values are calculated using Eq. (2). Eventually, the RSM models are formulated as follows, this RSM proxy model is used in the subsequent content to calculate FS and ω:

$$\begin{aligned}\omega = &-1.041\times10^{-3} + 1.73\times10^{-3}(A+B)\\ &+0.47\times10^{-3}(C+D) + 1.734\times10^{-11}E\\ &+8.671\times10^{-12}(F+G),\end{aligned} \tag{3}$$

$$
\begin{aligned}
FS = {} & -0.9228 + 0.191A + 0.0191B + 0.297C \\
& + 0.444D + 7.57\times10^{-8}E + 1.25\times10^{-8}F \\
& - 7.65\times10^{-8}G - 0.153AB - 0.048AC \\
& + 0.044AD + 1.62\times10^{-9}AE + 6.56\times10^{-10}AF \\
& + 3.96\times10^{-9}AG + 0.04BC - 0.074BD \\
& - 2.1\times10^{-9}BE - 2.09\times10^{-10}BF \\
& + 1.12\times10^{-8}BG - 0.043CD - 1.07\times10^{-8}CE \\
& + 6.67\times10^{-11}CF + 7.85\times10^{-9}CG \\
& - 1.1\times10^{-9}DE - 1.97\times10^{-9}DF \\
& - 5.95\times10^{-10}DG - 3.19\times10^{-16}EF \\
& + 8.69\times10^{-17}EG + 2.02\times10^{-16}FG \\
& - 0.033A^2 + 0.023B^2 - 6.4\times10^{-5}C^2 \\
& - 5.8\times10^{-4}D^2 - 6.54\times10^{-17}E^2 \\
& + 7.66\times10^{-17}F^2 + 4.41\times10^{-17}G^2.
\end{aligned} \tag{4}
$$

Since the ω values are calculated from data obtained from the equation and do not possess discrete characteristics, their correlation coefficient is 0.99. Therefore, only the *FS* model is tested using the complex correlation coefficients R^2 and adjusted complex correlation coefficients R^2_{adj}. A comparison graph illustrating the predicted values of the RSM model and the calculated values obtained from numerical simulation is plotted, as shown in Fig. 9.

The predicted values and simulated values are concentrated on both sides of the regression line and are uniformly distributed, with errors within 6%. The correlation coefficients of the response values are close to 1, and the difference between R^2 and R^2_{adj} is small, indicating that the fitting accuracy of this model is high.

5.2 Multiobjective optimization and evaluation

To minimize the overall construction cost while achieving maximum slope stability, the NSGA-II genetic algorithm is employed for multiobjective optimization analysis. In Section 5.2, two objective optimization functions are used: the mathematical models *FS*(*A*, *B*, *C*, *D*, *E*, *F*, *G*) and ω(*A*, *B*, *C*, *D*, *E*, *F*, *G*)) are established based on RSM to establish *FS* and ω concerning seven structural parameters. The multiobjective optimization mathematical model is formulated based on the objective functions and the range of variable values:

$$
\min \begin{Bmatrix} -FS(A,B,C,D,E,F,G) \\ \omega(A,B,C,D,E,F,G) \end{Bmatrix}, \tag{5}
$$

$$
s.t. \begin{Bmatrix} 0.6 \le (A,B) \le 2.4, (A,B) \in 0.1\times N, \\ 0.3 \le (C,D) \le 8.0, (C,D) \in 0.25\times N, \\ 1\times10^4 \le (E,F,G) \le 5\times10^4, \\ (E,F,G) \in 5\times\times10^3 N \end{Bmatrix}, \tag{6}
$$

where *N* is a natural number.

Setting up the more widely used particle swarm optimization algorithm for comparison with the NSGA-II algorithm. The algorithms is implemented using MATLAB for optimization analysis. After debugging, the population size is set to 200, the crossover probability is set to 0.8, the mutation probability is set to 0.08, and the maximum evolution generation is set to 200. Through NSGA-II multiobjective optimization, a set of Pareto optimal frontiers can be obtained, but a specific optimal parameter combination cannot be determined. Therefore, the weight distributions of *FS* and ω are first determined to be 53.43% and 46.57%, respectively, using the entropy weighting method. Then, the corresponding evaluation coefficients are calculated and ranked using the TOPSIS method. The obtained optimal Pareto solution set is shown in Fig. 10. The smoothness and uniformity of the Pareto solution set obtained by the particle swarm optimization algorithm is much smaller than that of NSGA-II, proving that it has poor diffusivity

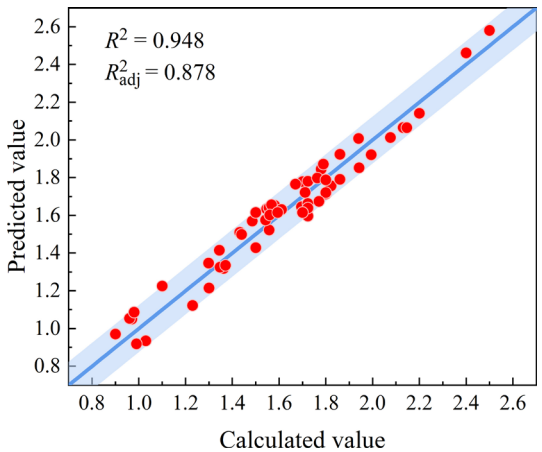

Fig. 9 Predicted value vs. calculated value of *FS*

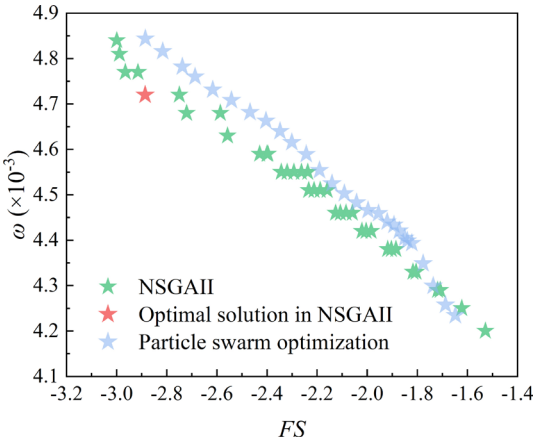

Fig. 10 Pareto solution set and optimal solution

in the feasible domain. Meanwhile, the ω of all the solutions obtained by the particle swarm optimization algorithm is higher than NSGA-II, and the FS are smaller than NSGA-II, so it can be considered that the optimization effect of NSGA-II algorithm is much stronger than that of the particle swarm algorithm.

The optimal structural parameters are as follows: beam length of 0.6 m, cantilever segment length of 0.7 m, rear pile length of 3 m, front pile length of 3 m, rear pile stiffness of 1×10^4 MPa, front pile stiffness of 1×10^4 MPa, and beam stiffness of 5×10^4 MPa. The slope stability coefficient under the optimal structural parameters is 2.886, which is 47.39% higher than the baseline value (1.958). The cost is 0.434 (these data are obtained by normalizing the optimal and baseline parameters), which is 75.19% lower than the baseline value of 1.749. The performance of the structure has significantly improved compared to before optimization, indicating that the RSM-NSGA-II method can effectively optimize the h-type anti-slide pile structure with remarkable results.

6 Conclusion

In this paper, structural optimization of the h-type anti-slide pile was carried out by RSM combined with NSGA-II, and the main conclusions were obtained as follows:

1. The bending moment distribution of the h-type anti-slide pile is obtained through indoor model tests and numerical simulations: the bending moment along the height of the rear pile exhibits an "inverted S-shaped" distribution, while the bending moment of the front pile increases first and then decreases from the bottom to the top of the pile. The distribution of soil pressure shows that the maximum pile front soil pressure of the rear pile occurs at the bottom of the pile, and the pile front soil pressure of the front pile approaches zero at the top of the pile.
2. The sensitivity of the structural parameters of the h-type anti-slide pile varies in terms of the reinforcement effect on the slope and the engineering cost. Almost all parameters have an impact on both the slope reinforcement effect and the engineering cost, and their influence increases with the increase in the parameters. The length of the cantilever segment has the most significant influence on the slope safety factor, while the stiffness of the rear pile has the most significant influence on the engineering cost.
3. The second-order RSM is suitable for establishing mathematical models that relate the parameters of the h-type anti-slide pile to the safety factor and cost, providing a high degree of fit. Using the RSM-NSGA-II method for optimization instead of finite element analysis can save a considerable amount of time and simultaneously consider the optimal cost and safety factor as multiple objectives, demonstrating high practical value.
4. Compared to NSGA-II, the particle swarm optimization algorithm is less diffuse in the feasible domain, and the optimization effect of NSGA-II is much stronger than that of the particle swarm optimization algorithm.
5. By combining the entropy weighting method and the TOPSIS method, the optimal solution in the Pareto solution set can be obtained conveniently. The optimized solution for the h-type anti-slide pile is as follows: H_{CB} = 0.6 m, H_{PB} = 0.7 m, H_{BP} = 3 m, H_{FP} = 3 m, $E_{BP} = 1 \times 10^4$ MPa, $E_{FP} = 1 \times 10^4$ MPa, $E_{CB} = 5 \times 10^4$ MPa. Compared to before optimization, the safety factor increased by 47.39%, and the cost decreased by 75.19%.

The limitations of this study primarily stem from the limited data collected during model test, which resulted in some data being insufficiently compared with finite element results. Additionally, it should be noted that this research mainly considers the conditions of loess slopes in areas with good soil quality, and caution should be exercised when applying these conclusions to slopes with different soil or rock.

Nomenclature

RSM	Response Surface Methodology
C_L	Geometric dimension similarity ratio
C_γ	Gravity similarity ratio
C_ε	Strain similarity ratio
C_σ	Stress similarity ratio
C_δ	Displacement similarity ratio
H_{CB}/A	Beam connection length
H_{PB}/B	Cantilever section length
H_{BP}/C	Rear row pile length
H_{FP}/D	Front row pile length
E_{CB}/G	Beam stiffness
E_{BP}/E	Rear row pile stiffness
E_{FP}/F	Front row pile stiffness

FS	Slope stability coefficient
ω	Cost of h-type anti-slide pile
R^2	Complex correlation coefficients
R^2_{adj}	Adjusted complex correlation coefficients

Acknowledgement

The research described in the paper was supported by National Natural Science Foundation of China (Nos.51878554) and Key Projects of Shaanxi Natural Science Basic Research Program (No. 2018JZ5012).

References

[1] Sun W., Liang, Q., Qiao, X., Cao, X., Wang, L. "Study on Dynamic Response of Loess Slopes with Different Failure Patterns", Journal of the China Railway Society, 44(06), pp. 123–130, 2022.

[2] Lei, D., Deng, P. Li, H., Luo, B., Zu, Z., Chen, Z. "Experimental Study on Dynamic Response of Bridge Pile Foundation Reinforced by Anti-Slide Pile on Landslide", China Railway Science, 2023, 44(02), pp. 73–82.

[3] Zhou, Y. "Research on mechanics effect of h-type anti-slide pile in slope treatment", MSc Thesis, Chongqing University, 2012.

[4] Sabri, M. M. S., Vatin, N. I., Ponomarev, A. B., Nurmukhametov, R. R., Kostyukov, I. I. "Settlement of Soil Reinforced with Vertical Fiberglass Micro-Piles", Materials, 15(14), 4744, 2022. https://doi.org/10.3390/ma15144744

[5] Deng Y.-S., Peng, C.-P., Liu, J.-C., Li, L.-T., Fu, Y.-B. "Optimization and Mechanical Characteristics of Spatial Arc Antislide Pile", Advances in Civil Engineering, 2021(1), 6508675, 2021. https://doi.org/10.1155/2021/6508675

[6] Shen Y.-j., Deng, B., Yang, Zheng, M.-y., Li, Y.-z., Cui, H.-h. M. "Elastoplastic models and calculation analysis of portal double-row anti-slide piles", Rock and Soil Mechanics, 35(S1), pp. 149–155, 2014. [online] Available at: http://ytlx.whrsm.ac.cn/EN/Y2014/V35/IS1/149 [Accessed: 25 August 2023]

[7] Ou, X., Tang Y., Cui, W., Li, J., Pan, X. "Model test and numerical simulation of h-type anti-slide pile", Chinese Journal of Rock Mechanics and Engineering, 31(9), pp. 1936–1943, 2012.

[8] Luo Y., Jiang, B., Li, C. "Research on the deformation and internal force characteristics of h-type anti-slide piles in landslide treatment", Chinese Journal of Underground Space and Engineering, 13(6), pp.1702–1710, 2017.

[9] Li, Y.-h. Zhang, X., Zhang, D.-h., Wang, W.-z. "Model test on mechanical behavior of h-type anti-slide pile under curved landslide", Engineering Mechanics, 40, pp. 1–13, 2022. https://doi.org/10.6052/j.issn.1000-4750.2022.05.0498

[10] Liu, X.-R., Kou, M.-M., Feng, H., Zhou, H. "Experimental and numerical studies on the deformation response and retaining mechanism of h-type anti-slide piles in clay landslide", Environmental Earth Sciences, 77(5), 163, 2018. https://doi.org/10.1007/s12665-018-7360-3

[11] Zhao, B., Wang, Y.-S., Wang Y., Shen, T., Zhai, Y.-C. "Retaining mechanism and structural characteristics of h type anti-slide pile (hTP pile) and experience with its engineering application", Engineering Geology, 222, pp. 29–37, 2017. https://doi.org/10.1016/j.enggeo.2017.03.018

[12] Zhao, L., Liao, W., Li. L., Shihong, H. "Improved calculation method for the internal force of h-type prestressed anchor cable antislide piles", International Journal of Geomechanics, 22(11), 04022187, 2022. https://doi.org/10.1061/(ASCE)GM.1943-5622.0002525

[13] Zhang, H., Xing, H.-F., Tannant, D., Xue D. "Centrifuge and numerical modeling of h-type anti-slide pile reinforced soil-rock mixture slope", Journal of Mountain Science, 20(5), pp. 1441–1457, 2023.

[14] Deng, Y., Zhang, K., Yao, Z., Zhao, H., Li, L. "Parametric analysis and multi-objective optimization of coupling beam-pile structure foundation", Ocean Engineering, 280, 114724, 2023. https://doi.org/10.1016/j.oceaneng.2023.114724

[15] Tang, H., Gong, W., Wang, L., Juang, C. H., Martin, J. R., Li, C. "Multiobjective optimization-based design of stabilizing piles in earth slopes", International Journal for Numerical and Analytical Methods in Geomechanics, 43(7), pp. 1516–1536, 2019. https://doi.org/10.1002/nag.2926

[16] Yao, W., Li, C., Zhan, H., Chen, W. "Probabilistic multi-objective optimization for landslide reinforcement with stabilizing piles in Zigui Basin of Three Gorges Reservoir region, China", Stochastic Environmental Research and Risk Assessment, 34(6), pp. 807–824, 2020. https://doi.org/10.1007/s00477-020-01800-5

[17] Deb, K., Agrawal, S., Pratap, A., Meyarivan, T. "A Fast Elitist Non-dominated Sorting Genetic Algorithm for Multi-objective Optimisation: NSGA-II", In: International Conference on Parallel Problem Solving From Nature, Paris, France, 2000, pp. 849–858. ISBN 978-3-540-41056-0 https://doi.org/10.1007/3-540-45356-3_83

[18] Xin, J., Tang, X., Zheng, Y., Dong, Z. "Large-scale model tests of single-row and triple-row anti-slide micropiles", Rock and Soil Mechanics, 36(4), pp. 1050–1056, 2015.

[19] Zhu, B., Pei, H., Yang, G. "An intelligent response surface method for analyzing slope reliability based on Gaussian process regression", International Journal for Numerical and Analytical Methods in Geomechanics, 43(15), pp. 2431–2448, 2019. https://doi.org/10.1002/nag.2988

[20] Jiang, H., Liu, B., Wang, Y., Zheng, S. "Multiobjective TOU Pricing Optimization Based on NSGA2", Journal of Applied Mathematics, 2014(1), 104518, 2014. https://doi.org/10.1155/2014/104518

[21] Wang Y., Liu, P., Yao, Y. "BMW-TOPSIS: A generalized TOPSIS model based on three-way decision", Information Sciences, 607, pp. 799–818, 2022. https://doi.org/10.1016/j.ins.2022.06.018

[22] Chen, P. "A Novel Coordinated TOPSIS Based on Coefficient of Variation", Mathematics, 7(7), 614, 2019. https://doi.org/10.3390/math7070614

[23] Anand, K., Elangovan, S. "Optimizing the ultrasonic inserting parameters to achieve maximum pull - Out strength using response surface methodology and genetic algorithm integration technique", Measurement, 99, 145–154, 2017. https://doi.org/10.1016/j.measurement.2016.12.025